Food and Chemical Toxicology 140 (2020) 111303

Contents lists available at ScienceDirect

Food and Chemical Toxicology

journal homepage: www.elsevier.com/locate/foodchemtox

Development of an adverse outcome pathway for cranio-facial malformations: A contribution from *in silico* simulations and *in vitro* data

Francesca Metruccio[a,1], Luca Palazzolo[b,1], Francesca Di Renzo[c], Maria Battistoni[b], Elena Menegola[c,*], Ivano Eberini[d], Angelo Moretto[b]

[a] ICPS, ASST Fatebenefratelli Sacco, via GB Grassi, 74- 20159, Milan, Italy
[b] Department of Biomedical and Clinical Sciences "L. Sacco", via GB Grassi 74- 20159, Milan, Italy
[c] Università degli Studi di Milano, Department of Environmental Science and Policy, via Celoria 26- 20133, Milan, Italy
[d] Università degli Studi di Milano, Department of Pharmacological and Biomolecular Sciences & DSRC, via Balzaretti 9- 20133, Milan, Italy

ARTICLE INFO

Keywords:
AOP
Malformation
In vitro
Docking
CYP26
HDAC

ABSTRACT

Mixtures of substances sharing the same molecular initiating event (MIE) are supposed to induce additive effects. The proposed MIE for azole fungicides is CYP26 inhibition with retinoic acid (RA) local increase, triggering key events leading to craniofacial defects. Valproic acid (VPA) is supposed to imbalance RA-regulated gene expression trough histone deacetylases (HDACs) inhibition. The aim was to evaluate effects of molecules sharing the same MIE (azoles) and of such having (hypothetically) different MIEs but which are eventually involved in the same adverse outcome pathway (AOP). An *in silico* approach (molecular docking) investigated the suggested MIEs. Teratogenicity was evaluated *in vitro* (WEC). Abnormalities were modelled by PROAST software. The common target was the branchial apparatus. *In silico* results confirmed azole-related CYP26 inhibition and a weak general VPA inhibition on the tested HDACs. Unexpectedly, VPA showed also a weak, but not marginal, capability to enter the CYP 26A1 and CYP 26C1 catalytic sites, suggesting a possible role of VPA in decreasing RA catabolism, acting as an additional MIE. Our findings suggest a new more complex picture. Consequently two different AOPs, leading to the same AO, can be described. VPA MIEs (HDAC and CYP26 inhibition) impinge on the two converging AOPs.

1. Introduction

Craniofacial malformations represent more than one-third of all congenital birth defects (cleft lip and/or palate alone or associated with other cranio-facial deformities, 1:700 live births; cranio-facial anomalies other than cleft lip and palate, 1:1600 newborns) (Mossey et al., 2009).

Craniofacial defects have a multifactorial etiology, involving both genetic (Twigg and Wilkie, 2015) and environmental risk factors (Mossey et al., 2009.). Some risk factors inducing cranio-facial defects have been identified, such as maternal active and passive smoking (Mossey et al., 2011)' (Sabbagh et al., 2015), alcohol consumption (Burns et al., 1974), Western-type diet (Vujkovic et al., 2007), maternal diabetes (Spilson et al., 2001), use of medicaments, such as some antiepileptic drugs (Nguyen et al., 2009)' (Alsaad et al., 2015) and retinoids (Suuberg, 2019), exposure to certain pesticides (Romitti et al., 2007) during the first trimester of pregnancy. There are indications that combined exposure to certain risk factors, such as alcohol and tobacco, have additive effects (Goncalves Leite and Koifman, 2009).

Craniofacial development entails a complex three-dimensional morphogenetic process, regulated by the morphogen retinoic acid (RA). A specific relationship has been described between RA gradient in different hindbrain areas, Hox gene expression, neural crest cells migration, pharyngeal arch formation and facial morphogenesis (Osumi-Yamashita, 1996) (Fig. 1). Pharyngeal arches (branchial arches, BAs) are symmetrical transient structures common to vertebrates at their phylotypic stage. The first BA (oral) is organized in an anterior maxillary process and in a posterior ventral mandibular process; normally the second BA (hyoid) appears well separated from the first (Fig. 1). A wide spectrum of craniofacial defects (among them: hemifacial microsomia, mandibulofacial dysostosis, branchio-oto-renal syndrome, Pierre Robin sequence and Nager acrofacial dysostosis) are classified as first

* Corresponding author.
E-mail addresses: metruccio.francesca@asst-fbf-sacco.it (F. Metruccio), luca.palazzolo@unimi.it (L. Palazzolo), francesca.direnzo@unimi.it (F. Di Renzo), maria.battistoni@unimi.it (M. Battistoni), elena.menegola@unimi.it (E. Menegola), ivano.eberini@unimi.it (I. Eberini), angelo.moretto@unimi.it (A. Moretto).
[1] These authors contributed equally to this work.

https://doi.org/10.1016/j.fct.2020.111303
Received 12 February 2020; Received in revised form 19 March 2020; Accepted 21 March 2020
Available online 03 April 2020

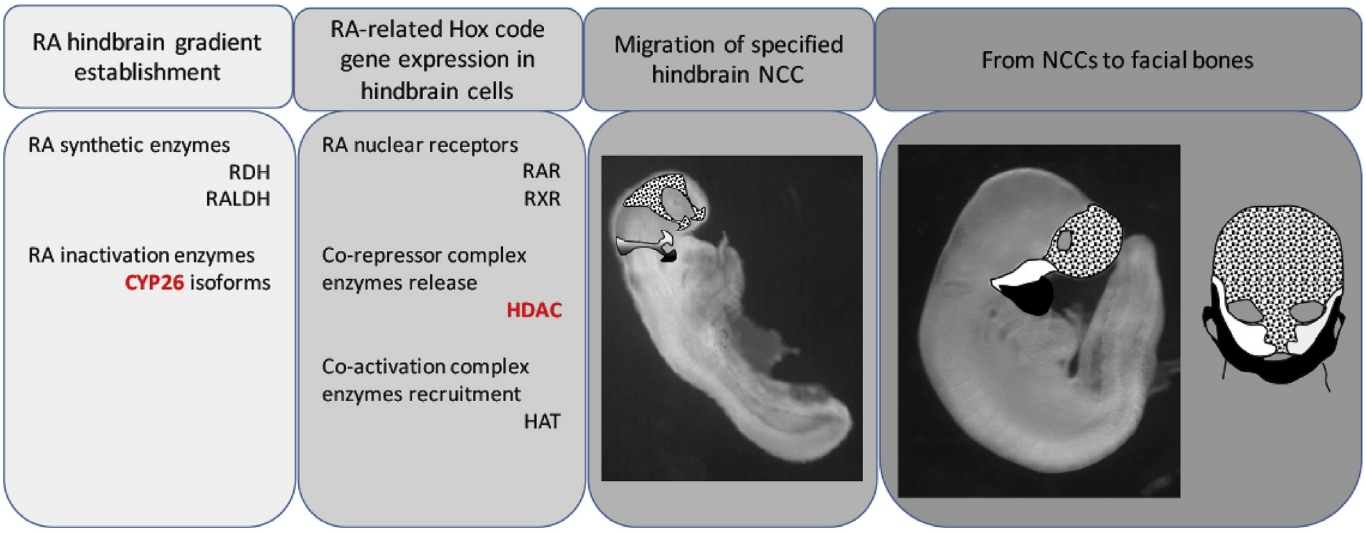

Fig. 1. Morphogenetic events involved in craniofacial development. The morphogenic pathway leads to the formation of specified NCCs migrating at the level of fronto-nasal process and into distinct branchial arches. In particular, the first branchial arch is crucial for facial skeletal organization and is subdivided into a maxillary process (white) also responsible for secondary palate organization and into a mandibular process (black). Dotted the fronto-nasal elements.
RA = retinoic acid; RDH = retinol dehydrogenase; RALDH = retinaldehyde dehydrogenase; RAR/RXR = retinoic acid nuclear receptors; HDAC = histone deacetylase; HAT = histone acetyltransferase; NCCs = neural crest cells.

and second branchial arch syndromes (Senggen et al., 2011). It has been shown that excessive RA concentrations at the time of facial morphogenesis leads to facial malformations (Lammer et al., 1985). RA gradient formation and maintenance are ensured by the correct equilibrium between RA synthesis and inactivation by CYP26 isoforms (Oosterveen et al., 2004). The Hox gene regulation machinery includes the histone deacetylase enzyme (HDAC, mainly the isoform HDAC7), associated with the co-repressor complex (Minoux and Rijli, 2010) (Fig. 1).

Making reference to molecular sequences in normal morphogenesis, it is possible to draw a hypothetical adverse outcome pathway (AOP). AOP describes a framework of information about the progression of toxicity events, starting from one or more molecular initiating events (MIEs), that trigger a sequence of biological events (key events, KEs) and leading to the final apical adverse outcome (AO). Within this scheme, different chemicals that switch on the same MIE can trigger the same KEs cascade and contribute to the same AO; also, switching a different MIE can trigger the same or partially overlapping cascade of KEs that leads to the same AO (Bal-Price et al., 2017). Finally, the scientifically-based description of the proposed AOPs could be also useful to better understand the pathogenesis of craniofacial defects related to genetic syndromes as well, contributing also to identify relevant gene polymorphisms that might increase the susceptibility to environmental factors for malformations, that appear to be mostly multifactorial. Also, understanding the dismorphogenic pathways would help in the discovery of those environmental factors that may contribute to the incidence of malformations. Based on a critical match between known or hypothesized molecular interactions of some chemicals, that induce facial defects, and relevant KEs for facial morphogenesis an AOP is proposed and shown in Fig. 2.

In detail, specific RA-like teratogenic effects at the level of the branchial structures were correlated to exposure to certain antifungal azoles, when tested in the post-implantation rat whole embryo cultures (WEC) (Di Renzo et al., 2019). The suggested hypothetical pathogenic pathway for azoles, which includes CYP26 inhibition as MIE (Menegola et al., 2006), was the basis for developing a quantitative AOP for craniofacial malformations (Battistoni et al., 2019).

Antiepileptic drugs, including valproic acid (VPA), are correlated to multiple malformations (neural tube, cardiac, craniofacial, skeletal and limb defects) classified as Fetal Valproate Syndrome (Ornoy, 2009; Weston et al., 2016). As far as axial skeletal defects are concerned, a direct relationship with HDAC inhibition was previously suggested (Menegola et al., 2005b), while no MIEs have been identified for other VPA-related teratogenic outcomes, including facial defects.

The aims of the present work are to: 1) investigate, in more detail, the suggested AOP outlined in Fig. 2; 2) to rank the relative potencies of some chemicals, associated with craniofacial defects in humans, using the WEC *in vitro* method; 3) investigate the suggested MIEs, matching the *in vitro* results with *in silico* approaches. Clarifying an AOP and defining quantitative KE relationships will be helpful in devising experimental studies with appropriate end-point measurements, e.g. to assess the combined effects of exposure to chemicals triggering different MIEs but leading to the same AO. In particular, these experiments are needed to assess to what extent and in which conditions dose-additivity for such compounds does apply. In fact, while it is biologically plausible that, once activated the common KE, co-exposure will add on the effect, the question would be whether at environmentally relevant exposures i.e. at doses not triggering the AOP cascade the addition will or will not occur.

The molecules selected for the *in silico* and *in vitro* experiments are three azole pesticides (triadimefon, FON, cyproconazole, CYPRO, and flusilazole, FLUSI), the histone deacetylases inhibitor valproic acid (VPA), and RA (as reference molecule). Among those previously characterized (Di Renzo et al., 2019), the selected azoles are known to induce both branchial defects *in vitro* (Menegola et al., 2000, 2001; Di Renzo et al., 2011). Moreover in regulatory studies on developmental toxicity, assessed in the frame of EU registration, cyproconazole and flusilazole showed facial defects, in particular cleft palate in rats, after *in utero* exposure (EFSA, 2010; JMPR, 2010; JMPR, 2007). Additionally, administration of FON to pregnant animals, showed increased fetal incidence of cleft palate in rats and rabbits (JMPR, 2004) and mice (Menegola et al., 2005a). RA and VPA are related to dysmorphogenic effects, including branchial defects *in vitro* (Gofflot et al., 1996; Di Renzo et al., 2019) and to facial dysmorphology in humans (Lammer et al., 1985; DiLiberti et al., 1984).

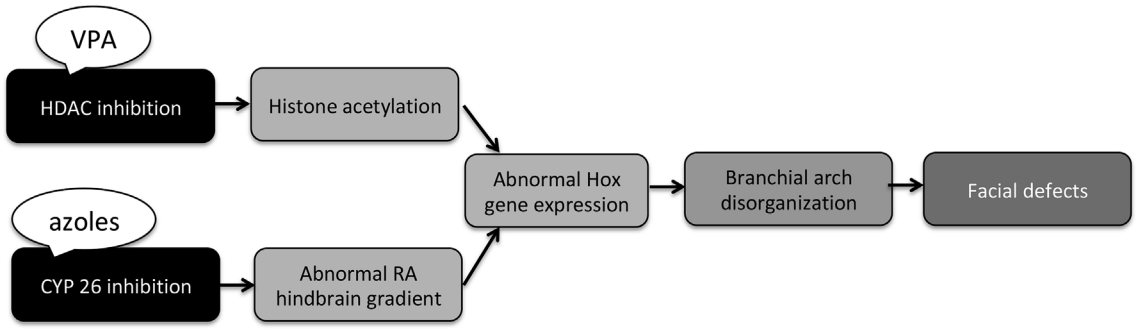

Fig. 2. Hypothetical adverse outcome pathways (AOPs) confluent to the same adverse outcome (AO, facial defects). The tested azoles (FON, CYPRO, FLUSI) and valproic acid (VPA), causing different molecular initiating events (MIEs, black), hypothetically trigger key events (KEs, grey) leading to the common adverse outcome (AO, dark grey).

2. Materials and methods

2.1. WEC

2.1.1. Materials and compound preparation

The medium used for the extraction of embryos from the uteri was sterilized Tyrode solution (Sigma); the medium used for the post-implantation whole embryo culture was undiluted heat inactivated rat serum added with antibiotics (penicillin 100 IU/mL culture medium and streptomycin 100 µg/mL culture medium, Sigma). All the tested compounds were purchased by Sigma, Italy (PESTANAL®, analytic grade). Azoles (FON, CYPRO, FLUSI, dissolved in ethanol in order to reach the final ethanol concentration in the medium equal to 17.35 mM), RA (dissolved in DMSO), VPA (Sodium Valproate, dissolved in Tyrode) were added to the culture medium in order to reach the final concentration of the different experimental groups (Fig. 3). For each dose-response experiment, a group exposed to the relevant solvent (dose 0) was prepared.

2.1.2. Embryo culture

All animal use protocols were approved by the Ministry of Health - Department for Veterinary Public Health, Nutrition and Food Safety committee. In compliance with EU Directive 2010/63/EU, animals were treated humanely and with regard for alleviation of suffering. Virgin female CD:Crl rats (Charles River, Calco, Italy), housed in a thermostatically maintained room (T = 22 ± 2 °C; relative humidity 55 ± 5%) with a 12 h light cycle (light from 6.00 a.m. to 6.00 p.m.), free access to food (Italiana Mangimi, Settimo Milanese, Italy) and tap water, were caged overnight with males of proven fertility. Embryos were explanted from untreated pregnant rats at E9.5 (early neurula stage, 1–3 somites; day of positive vaginal smear = 0) and cultured according to the New's method (New, 1978) in 20 ml glass bottles (5 embryos/bottle), containing 5 mL culture medium and test molecules at different concentrations. The bottles, inserted in a thermostatic

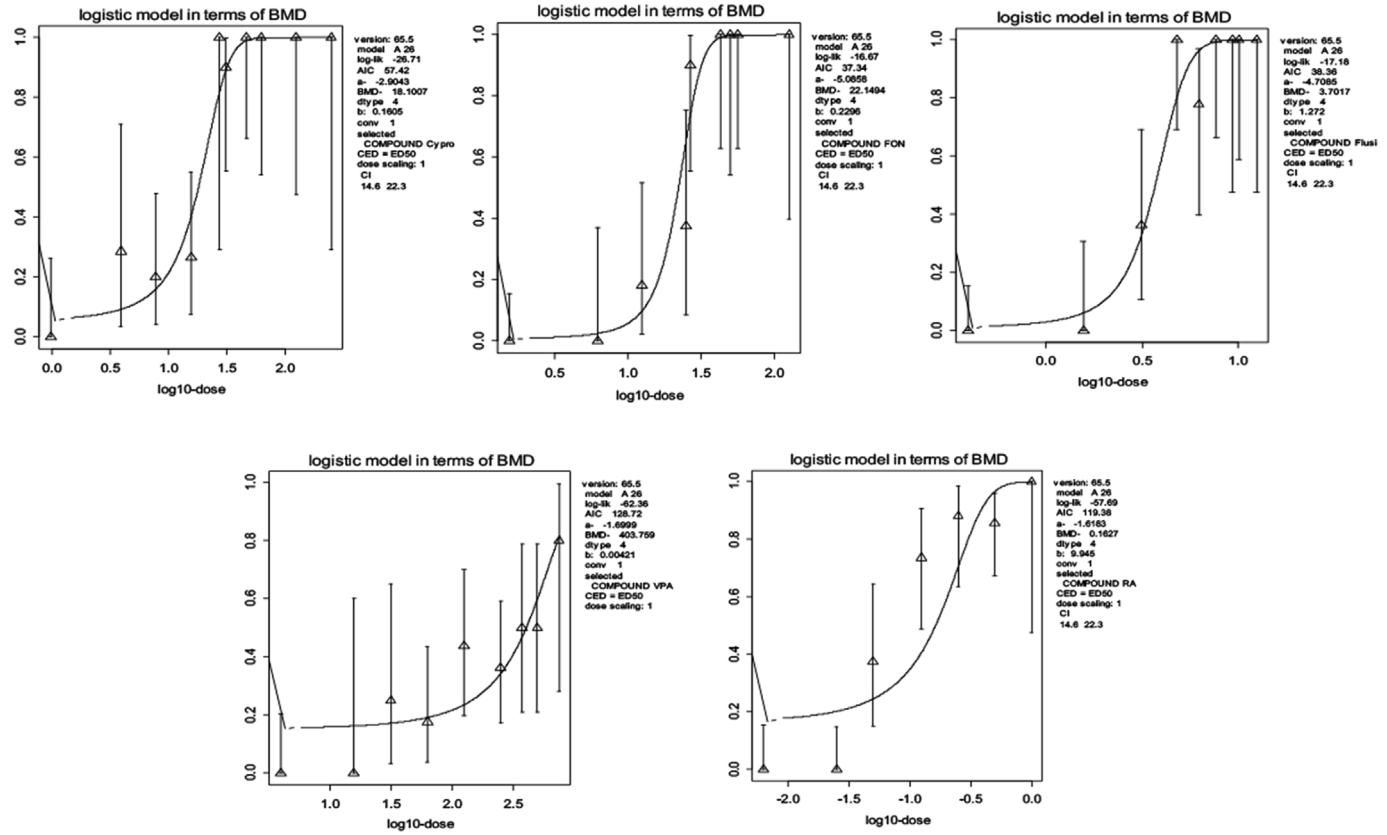

Fig. 3. Single dose-response curves. CYPRO, FON, FLUSI, VPA and RA were modelled in terms of benchmark dose (BMD) using PROAST software.

(37.8 °C) roller (30 rpm) apparatus, were periodically gas equilibrated according to Giavini et al. (1992) (Giavini et al., 1992). After 48 h of culture, embryos were morphologically examined under a dissecting microscope in order to evaluate any branchial or extra-branchial abnormality. At least a triplicate was performed for each group.

2.1.3. Data analysis

Statistical evaluation was applied on frequencies (chi-square test for multiple comparison), setting the level of significance at $p < 0.05$.

PROAST analysis (65.5 version) was applied on branchial outcomes, because this apparatus was the common target for all the tested substances and the target of the present study. Data were modelled to obtain the single dose-response curves (from these curves, the benchmark doses at 50% - BMR50) and the relative potency factors (RPFs, RA being the reference compound).

2.2. Molecular modeling

The primary structures of the selected rat enzymes were downloaded from the UniProt Protein Knowledgebase database ("UniProt,"). After a protein BLAST search of the RCSB Protein Data Bank (PDB) database ("RCSB PDB: Homepage,") for homologues to the selected enzymes, the crystallographic structures reported in Table 1 were set as templates, downloaded from the PDB and structure-prepared using the Structure Preparation program of the MOE 2019.01 suite (Chemical Computing Group), in order to address any crystallographic issues and to add missing atoms/residues. All the alignments were produced through the Clustal Omega software ("Clustal Omega < Multiple Sequence Alignment < EMBL-EBI,") and manually checked. All the comparative models were produced by the MOE Homology Model program of the Protein module with default settings, also importing both the ligand and the cofactor co-crystallized with the template enzymes. The quality of the final models was carefully checked with the MOE Protein Geometry program.

The catalytic sites of the selected enzymes were identified through the MOE Site Finder program, which uses a geometric approach to list putative binding sites in a protein, starting from its three-dimensional structure. The correspondence with the co-modelled ligand was then carefully checked.

Selected chemicals were downloaded from the PubChem database ("PubChem,"). Each entry was converted into a three-dimensional structure, and energy minimized, with the MOE Energy Minimize program, down to a RMS gradient of 0.05 kcal/mol/Å^2. Stereochemistry of each structure was carefully checked. Molecular docking was carried out through the MOE Dock program. The Triangle Matcher placement algorithm was used for exploring only the enzyme catalytic site, and the London dG empirical scoring function was applied for sorting the poses. The 30 top-scoring poses were refined through molecular mechanics, considering each receptor as a rigid body, and the refined complexes were scored through the GBVI/WSA dG empirical scoring function, selecting the five top-scoring poses. All the co-modelled ligands were used for validating the molecular docking procedure on 3-D models, obtaining docking poses that are compliant with the original structures.

3. Results

3.1. WEC

All tested molecules induced concentration-related branchial defects (BA fused, Table 2); RA and VPA induced multiple district anomalies including extra-branchial abnormalities (neural tube defects, somite abnormalities, hook-shaped tail).

PROAST analysis on branchial outcomes was first performed in order to compare the fit to the single dataset (Fig. 3) with the fit to the combined dataset (Fig. 4), using in both cases exponential model family tests. As the log-likelihood ratio test did not reject the equal steepness assumption ($p = 0.88$ with log-likelihood of separate fits $= -180.61$, log-likelihood of the overall fit $= -182.12$, degrees of freedom $= 7$) (Table 3), the benchmark doses (BMDs) for benchmark response (BMR) at 50% and relative potency factors (RPFs) were estimated using the combined model fit (Figs. 4 and 5). The evaluation of CIs of RPFs suggests potency ranking as follow: RA > FLUSI > CYPRO/FON > VPA (Fig. 6). Even if FLUSI resulted at least one order of magnitude less potent than RA, it resulted nearly one order of magnitude more potent than the other tested azoles. VPA was the less potent of all, at least four orders of magnitude less potent than RA.

3.2. Docking

Table 4 shows the binding free energies of the chemicals docked into the selected enzymes. As expected, RA (the natural CYP26 substrate) is the best CYP26 isoenzymes ligand, since it shows the best ΔG with respect to the other tested chemicals, and, according to its binding free energy (ΔG) values, it is possible to classify RA as a strong binder of the three CYP26 isoenzymes. Azoles, with a comparable ΔG value for each CYP26 isoenzyme, can be classified as good ligands, while VPA, with the least negative ΔG values for the three CYP26 isoenzymes, can be classified as a weak ligand.

All the binding poses were carefully checked, pointing out that in each CYP26 isoenzyme all the selected chemicals are located near the heme Fe^{2+} ion. In particular, all the RA binding poses are comparable with the placement of the co-modelled RA (Fig. 7A), while all the azoles show the azolic ring exposed to the heme group, in agreement with Pautus and colleagues (Pautus et al., 2009). VPA can accommodate itself in the CYP26 isoenzyme binding sites in two different modes: in the first, observed for CYP26A1 and CYP26C1, VPA is close to the heme group, while in the second, observed for CYP26B1, VPA is far from the catalytic site (Fig. 7B), suggesting that VPA is not a ligand for this isoenzyme.

On the contrary, VPA may be classified as ligand of HDAC isoenzymes, whereas RA could be only hypothesized as a putative weak interactor. In fact, VPA binds a very deep region of the catalytic site, near the Zn^{2+} ion. According to Sixto-López et al., (2014) (Sixto-López

Table 1
Reference structures for homology modelling the selected proteins involved in MOAs craniofacial malformations.

Protein	UniProtKB code	Template	RCSB PDB code	Identity percent	Reference
CYP26A1_RAT	**G3V861**	**CP120_SYNY3**	**2VE3**	**34.8%**	[39]
CYP26B1_RAT	**G3V7X8**	**CP120_SYNY3**	**2VE3**	**35.1%**	[39]
CYP26C1_RAT	**D4AAL3**	**CP120_SYNY3**	**2VE3**	**33.5%**	[39]
HDAC1_RAT	**Q4QQW4**	**HDAC1_HUMAN**	**4BKX**	**99.2%**	[40]
HDAC2_RAT	**B1WBY8**	**HDAC2_HUMAN**	**4LY1**	**99.0%**	[41]
HDAC3_RAT	**Q6P6W3**	**HDAC3_HUMAN**	**4A69**	**99.8%**	[42]
HDAC4_RAT	**Q99P99**	**HDAC4_HUMAN**	**2VQM**	**93.4%**	[43]
HDAC7_RAT	**A0A0G2K6B1**	**HDAC7_HUMAN**	**3C10**	**92.4%**	[44]
HDAC8_RAT	**B1WC68**	**HDAC8_HUMAN**	**5DC5**	**96.3%**	[45]
HDAC10_RAT	**E5RQ38**	**HDAC5_HUMAN**	**5TD7**	**57.5%**	[46]

Table 2
Percentage of embryos with malformations at the branchial arches (BA).
Grey columns indicate concentration levels at witch extra-branchial defects were also observed.

RETINOIC ACID	RA 0 μM	RA 0.025 μM	RA 0.05 μM	RA 0.125 μM	RA 0.25 μM	RA 0.5 μM	RA 1 μM
BA abnormalities	0.0	0.0	37.5	73.7	88.2	85.7	100.0
CYPROCONAZOLE	CYPRO 0 μM	CYPRO 3.9 μM	CYPRO 7.8 μM	CYPRO 15 μM	CYPRO 31 μM	CYPRO 46.8 μM	CYPRO 62.5 μM
BA abnormalities	0.0	28.6	20.0	22.2	90.0	100.0	100.0
FLUSILAZOLE	FLUSI 0 μM	FLUSI 1.56 μM	FLUSI 3.125 μM	FLUSI 4.8 μM	FLUSI 6.25 μM	FLUSI 7.7 μM	FLUSI 9.375 μM
BA abnormalities	0.0	0.0	36.4	100.0	77.8	100.0	100.0
TRIADIMEFON	FON 0 μM	FON 6.25 μM	FON 12.5 μM	FON 25 μM	FON 26.7 μM	FON 42.85 μM	FON 50 μM
BA abnormalities	0.0	0.0	18.2	37.5	90.0	100.0	100.0
VALPROIC ACID	VPA 0 μM	VPA 15.625 μM	VPA 31.25 μM	VPA 62.5 μM	VPA 125 μM	VPA 250 μM	VPA 375 μM
BA abnormalities	0.0	0.0	25.0	17.6	43.8	36.4	50

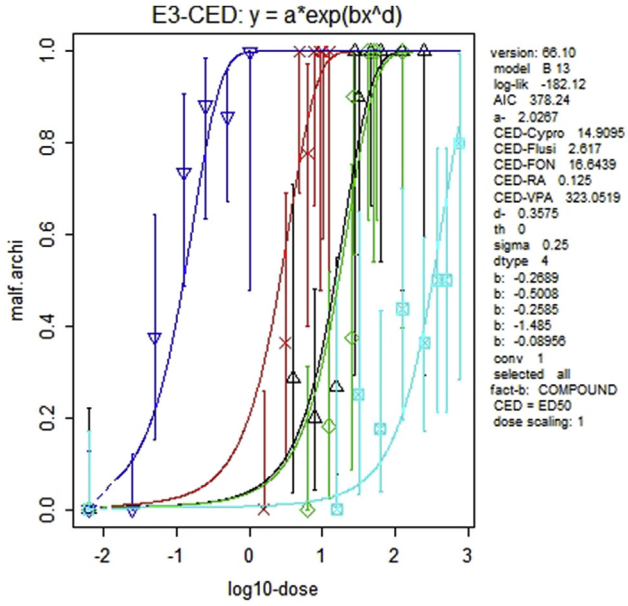

Fig. 4. Evaluation of the benchmark doses (BMDs) for benchmark response at 50% of CYPRO, FON, FLUSI, VPA in respect to RA. From left to right: RA-FLUSI-CYPRO-FON-VPA.

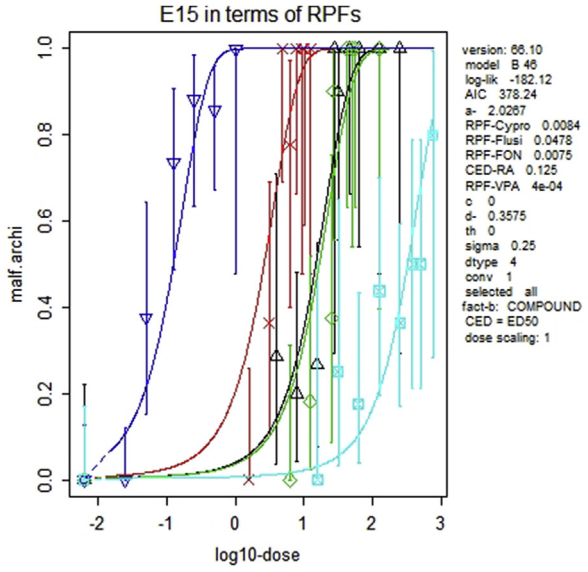

Fig. 5. Evaluation of the relative potency factors (RPFs) of the effects of CYPRO, FON, FLUSI, VPA in respect to RA. From left to right: RA-FLUSI-CYPRO-FON-VPA.

Table 3
Parameters obtained by PROAST analysis, fitting separate dataset for each compound and combined dataset for all. BMD = benchmark dose; BMR = benchmark response.

	BMD for BMR 50% (μM)	log-likelihood
RA	0.16	−57.69
CYPRO	18.1	−26.71
FON	22.15	−16.67
FLUSI	3.7	−17.18
VPA	403.8	−62.36
COMBINED (RA as index)	0.125	−182.12

et al., 2014) the carboxylic group of VPA establishes metal/ion interaction with Zn^{2+} in all the HDAC isoenzymes; moreover, the computed affinity (ΔG) of VPA for HDAC8 agrees with other *in silico* data (Bermúdez-Lugo et al., 2012). Differently, for each tested HDAC isoenzyme, the RA carboxylic group cannot interact with the Zn^{2+} ion, while the carbocyclic ring is not buried in the binding site, but partially exposed to the solvent. Differently, all the investigated azoles do not bind the catalytic site of tested HDACs. No azole establishes interaction with Zn^{2+} ion. For this reason, azoles cannot be classified as HDACs ligands.

4. Discussion

The aim of the present work was to rank the relative potencies of selected chemicals associated with craniofacial defects in humans and

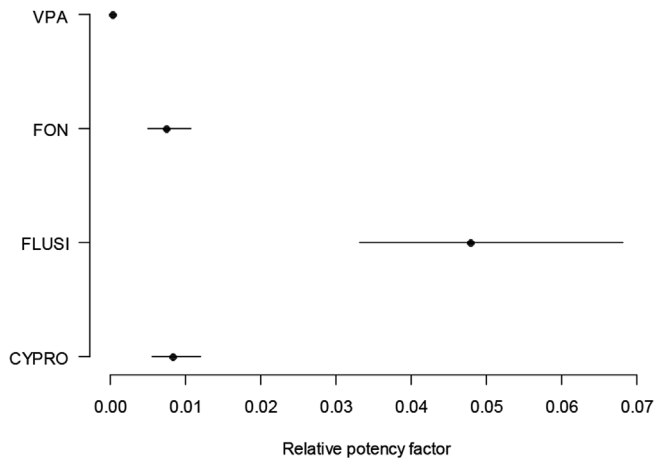

Fig. 6. Plot of relative potency factors (RPFs) with confidence intervals (CIs) considering RA potency = 1.

to investigate the suggested AOP shown in Fig. 2. Data obtained by *in vitro* exposure (WEC) to the different chemicals and modelled by PROAST analysis allowed potency ranking with RA more active, as expected. Azoles were less effective than RA (with the following ranking: FLUSI > CYPRO/FON) and VPA was even less active. The match between the *in vitro* results and *in silico* data showed a complex picture and unexpected results. In contrast to the initial hypothesis of different MIEs (CYP26 inhibition for azoles, HDAC inhibition for VPA) involved in inducing a similar adverse outcome (branchial defects, as observed after embryo evaluation), the *in silico* approach pointed out a more complex interaction network.

Literature data describe the time course of CYP 26 isozyme expression in rodent embryos. CYP 26A1 is initially expressed in the anterior neural plate during gastrulation (Kudoh et al., 2002) and later has a key role in the developing hindbrain to precisely restrict the field of endogenous RA signalling (White and Schilling, 2008). In contrast to CYP26A1, CYP26B1 expression appears later and is associated with a more dynamic pattern in the hindbrain. CYP26C1 initially appears in the head mesenchyme (Uehara et al., 2007), and is then expressed after gastrulation in specific hindbrain regions. Using Cyp26a1−/−Cyp26c1−/− mice, Uehara et al. (2007) suggested that the activity of CYP26A1 and CYP26C1 is required for correct neural antero-posterior patterning and production of migratory cranial neural crest cells colonizing craniofacial regions. Consistent with the hypothesis, that Cyp26a1−/−Cyp26c1−/− phenotype showed branchial abnormalities actually similar to those observed in our *in vitro* experiment.

Even if with an affinity lower than the natural substrate (RA), all the tested azoles can bind CYP26 isoenzymes with a significant predicted binding free energy, showing a well conserved binding mode, already described in literature (Pautus et al., 2009), in which the azolic ring is arranged close to the heme Fe^{2+} ion. Since no azole metabolites oxidized in the azolic ring have been reported, and since our binding poses do not satisfy geometrical restrain reported in Pautus and colleagues (Pautus et al., 2009) and mandatory for the enzymatic reaction, our data suggest that for CYP26 isoenzymes azoles are not substrates but competitive inhibitors. In contrast, as expected, RA is the only chemical that can establish a specific interaction with the heme group in all the three CYP26 isoenzymes.

Contrary to the earlier assumption regarding the ubiquitous expression of HDACs (Weichert, 2009), recent studies clearly demonstrated that also HDACs are expressed in space- and time-specific manner during development (Tab 5). As far as the craniofacial morphogenesis is concerned, a strong expression is described for HDAC1 and HDAC2 at the branchial arch level in mouse E10 embryos (Murko et al., 2010). As shown by Milstone et al. (2017) HDAC1 and HDAC2 are expressed in NCCs and their derivatives (including branchial arches) in mouse embryos and regulate branchial arch formation. HDAC1 and HDAC2 have already been supposed to be implicated in congenital craniofacial defects seen in humans (Hudson et al., 2014; De Souza et al., 2015; Matsumoto et al., 2015) In addition, HDAC8 seems to regulate skull morphogenesis only during late gestation, confirming a unique role of HDAC1 and HDAC2 within early craniofacial embryogenesis (Haberland et al., 2009). Furthermore, expression in multiple extra cranio-facial districts (including the developing brain) was described for a number of HDACs (HDAC1, HDAC2, HDAC3, HDAC8) in E10 mouse embryos (Murko et al., 2010), whereas, consistent with HDAC7 null mice phenotype, HDAC7 expression in E9.5 mouse embryos was limited to the developing vascular endothelium (Tab 65) (Chang et al., 2006).

VPA is described as a weak HDAC inhibitor (Eckschlager et al., 2017) and this seems an interesting feature for repositioning this antiepileptic drug as anticancer (Eckschlager et al., 2017; Krauze et al., 2015; Suraweera et al., 2018). Its HDAC inhibitory capability was previously demonstrated also in mouse embryos nuclear extracts, suggesting a specific inhibitory activity on nuclear HDACs expressed during embryo development (Di Renzo et al., 2007).

In silico results on VPA-HDACs docking (Table 5) confirm a weak general inhibitory activity of VPA on the tested HDACs, including, but not exclusively, HDAC1 and 2. This activity on HDAC1 and 2 could be considered supportive for the corroboration as a MIE in VPA teratogenic effects.

Unexpectedly, VPA shows, in addition, a weak, but not marginal, capability to enter the CYP 26A1 and CYP 26C1 catalytic sites, suggesting a possible role of VPA in decreasing RA catabolism, but with a difference of approximatively two orders of magnitude in comparison with azoles. Approximated K_is, obtained from the binding free energy values, could be compatible with the tested active concentrations, and this could be considered at the basis of an additional MIE. Conversely, the binding free energy of RA suggests only a marginal role of this morphogen on HDAC activity that, if demonstrated, would become appreciable only at definitively higher concentrations than those tested and resulted teratogenic. These complex interactions could be related to the documented multilevel modulation of different RA-dependent gene activators. Together with the varying expression of the target enzymes in space and time, this could explain the malformations induced by VPA as well as by azoles.

Our findings thus suggest a new picture related to the evaluated AO including similar (azoles) and partially dissimilar (azoles-VPA)

Table 4
Binding free energy values of tested molecules. Values are express in kcal/mol.

Chemical	CYP 26A1	CYP 26B1	CYP 26C1	HDAC1	HDAC2	HDAC3	HDAC4	HDAC7	HDAC8	HDAC10
FLUSI	**−7.3**	**−7.0**	**−7.7**	[a]	[a]	[a]	[a]	[a]	[a]	[a]
FON	**−7.4**	**−7.5**	**−7.5**	[a]	[a]	[a]	[a]	[a]	[a]	[a]
CYPRO	**−7.2**	**−7.0**	**−7.5**	[a]	[a]	[a]	[a]	[a]	[a]	[a]
RA	**−8.9**	**−8.9**	**−10.2**	**−6.1**	**−5.7**	**−5.7**	**−5.4**	**−5.2**	**−6.1**	**−6.0**
VPA	**−5.6**	[a]	**−6.0**	**−4.9**	**−4.9**	**−3.1**	**−4.1**	**−4.1**	**−5.0**	**−4.4**

[a] These ligands bind far from the catalytic site (more details in the text).

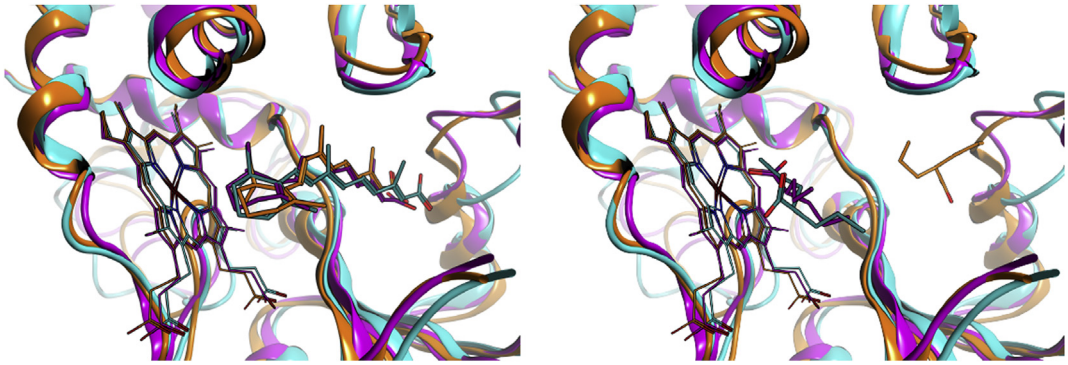

Fig. 7. Binding poses of RA (A) and VPA (B). CYP26A1, CYP26B1 and CYP26C1 are represented as blue, orange and violet ribbon, respectively. (For interpretation of the references to colour in this figure legend, the reader is referred to the Web version of this article.)

Table 5
Summary of HDAC expression during mouse E10 embryogenesis (corresponding to the rat stage at the end of the culture period).

ISOFORMS	EXPRESSION	Ref	ISOFORMS	Knockout phenotype	Ref
HDAC1	Brain, branchial arches, limb buds, otic vesicle	Murko et al. (2010)	HDAC1	Early death	Lagger et al. (2002), Montgomery et al. (2007)
HDAC2	Brain, branchial arches (distal)	Murko et al. (2010)	HDAC2	Cardiac defects/perinatal lethality	Montgomery et al. (2007), Trivedy et al. (2007)
HDAC3	Forebrain, midbrain, otic vesicle	Murko et al. (2010)	HDAC3	Early lethality; cardiovascular defects	Montgomery et al. (2008), Knutson et al. (2008)
HDAC8	Forebrain, midbrain	Murko et al. (2010)	HDAC8	Cranial defects related to specific cranial NCCs deficiency	Haberland et al. (2009)
HDAC7	Developing cardio-vascular tissues	Chang et al. (2006)	HDAC7	Vascular dilatation and rupture/midgestation death	Chang et al. (2006)

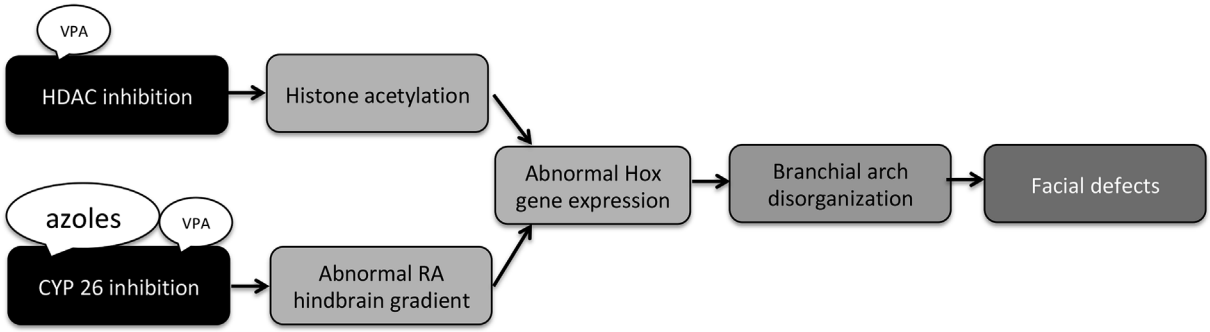

Fig. 8. Adverse outcome pathways (AOPs) leading to the same adverse outcome (AO, facial defects), as suggested by data of the present work. Both the tested azoles (FON, CYPRO, FLUSI) and valproic acid (VPA), even if with different affinity, are involved in CYP26 inhibition. VPA is also involved in HDAC inhibition. MIEs trigger different key events (KEs, grey) leading to a common KE (abnormal Hox gene expression) and, finally to the common adverse outcome (AO, dark grey).

molecular targets. Consequently two different AOPs, confluent on the same AO, can be described. While azoles seem to be involved in a linear pathway, VPA MIEs (HDAC and CYP26 inhibition) impinge on the two converging AOPs affecting craniofacial structures (Fig. 8).

5. Conclusions

The present tiered approach (*in silico* docking in order to evaluate hypothetical MIEs; *in vitro* WEC approach in order to obtain robust data to model) resulted adequate to improve the hypothetical AOP for craniofacial defects.

Interestingly, this approach confirmed the supposed MIEs but also suggested that at least an additional MIE can be considered to explain VPA-related craniofacial defects.

Future experiments on mixtures could be aimed in order to deep evaluate the effects of binary mixtures of azoles and VPA.

The present work assumes also a particular interest considering that RA pathways are currently an emerging issue in toxicology, and chemicals able to interfere with RA pathway have recently received more and more attention (Wu et al., 2014; Chen and Reese, 2016).

CRediT authorship contribution statement

Francesca Metruccio: Software, Validation, Formal analysis, Visualization, Writing - original draft. **Luca Palazzolo:** Validation, Formal analysis, Visualization, Writing - original draft. **Francesca Di Renzo:** Conceptualization, Validation, Investigation, Resources, Writing - original draft, Writing - review & editing. **Maria Battistoni:**

Data curation, Visualization. **Elena Menegola:** Conceptualization, Validation, Investigation, Writing - review & editing, Writing - original draft, Supervision. **Ivano Eberini:** Supervision. **Angelo Moretto:** Conceptualization, Validation, Supervision, Project administration, Writing - review & editing.

Declaration of competing interest

The authors declare that they have no known competing financial interests or personal relationships that could have appeared to influence the work reported in this paper.

Acknowledgements

This work was funded by H2020 Framework Programme of EU (EuroMix project).

Luca Palazzolo and Ivano Eberini were also supported by grants from Italian Ministry Project MIUR –Progetto Eccellenza; Ivano Eberini was also supported by National FABR 2017 (Fondo di Finanziamento pr l'Attività Base di Ricerca).

Appendix A. Supplementary data

Supplementary data to this article can be found online at https://doi.org/10.1016/j.fct.2020.111303.

References

Alsaad, A.M.S., Chaudhry, S.A., Koren, G., 2015. First trimester exposure to topiramate and the risk of oral clefts in the offspring: a systematic review and meta-analysis. Reprod. Toxicol. https://doi.org/10.1016/j.reprotox.2015.03.003.

Bal-Price, A., Meek, M.E., Bette, 2017. Adverse outcome pathways: application to enhance mechanistic understanding of neurotoxicity. Pharmacol. Ther. https://doi.org/10.1016/j.pharmthera.2017.05.006.

Battistoni, M., Di Renzo, F., Menegola, E., Bois, F.Y., 2019. Quantitative AOP based teratogenicity prediction for mixtures of azole fungicides. Comput. Toxicol. https://doi.org/10.1016/j.comtox.2019.03.004.

Bermúdez-Lugo, J.A., Perez-Gonzalez, O., Rosales-Hernández, M.C., Ilizaliturri-Flores, I., Trujillo-Ferrara, J., Correa-Basurto, J., 2012. Exploration of the valproic acid binding site on histone deacetylase 8 using docking and molecular dynamic simulations. J. Mol. Model. https://doi.org/10.1007/s00894-011-1240-z.

Burns, J.E., Miller, F.M., Gomes, E.D., Albert, R.A., 1974. Hexachlorobenzene exposure from contaminated dcpa in vegetable spraymen. Arch. Environ. Health 29, 192–194. https://doi.org/10.1080/00039896.1974.10666567.

Chang, S., Young, B.D., Li, S., Qi, X., Richardson, J.A., Olson, E.N., 2006. Histone deacetylase 7 maintains vascular integrity by repressing matrix metalloproteinase 10. Cell 126, 321–334. https://doi.org/10.1016/j.cell.2006.05.040.

Chen, Y., Reese, D.H., 2016. Disruption of retinol (Vitamin A) signaling by phthalate esters: SAR and mechanism studies. PloS One 11 (8), e0161167. https://doi.org/10.1371/journal.pone.0161167.

Clustal Omega < Multiple Sequence Alignment < EMBL-EBI [WWW Document].

De Souza, K.R., Mergener, R., Huber, J., Campos Pellanda, L., Riegel, M., 2015. Cytogenomic evaluation of subjects with syndromic and nonsyndromic conotruncal heart defects. BioMed Res. Int. https://doi.org/10.1155/2015/401941.

Di Renzo, F., Cappelletti, G., Broccia, M.L., Giavini, E., Menegola, E., 2007. Boric acid inhibits embryonic histone deacetylases: a suggested mechanism to explain boric acid-related teratogenicity. Toxicol. Appl. Pharmacol. https://doi.org/10.1016/j.taap.2007.01.001.

Di Renzo, F., Rossi, F., Prati, M., Giavini, E., Menegola, E., 2011. Early genetic control of craniofacial development is affected by the in vitro exposure of rat embryos to the fungicide triadimefon. Birth Defects Res. Part B Dev. Reproductive Toxicol. https://doi.org/10.1002/bdrb.20284.

Di Renzo, F., Metruccio, F., Battistoni, M., Moretto, A., Menegola, E., 2019. Relative potency ranking of azoles altering craniofacial morphogenesis in rats: an in vitro data modelling approach. Food Chem. Toxicol. https://doi.org/10.1016/j.fct.2018.12.004.

DiLiberti, J.H., Farndon, P.A., Dennis, N.R., Curry, C.J.R., 1984. The fetal valproate syndrome. Am. J. Med. Genet. https://doi.org/10.1002/ajmg.1320190308.

Eckschlager, T., Plch, J., Stiborova, M., Hrabeta, J., 2017. Histone deacetylase inhibitors as anticancer drugs. Int. J. Mol. Sci. 18, 1414. https://doi.org/10.3390/ijms18071414.

EFSA, 2010. Journal 8 (11), 1897 2010.

Giavini, E., Broccia, M.L., Prati, M., Bellomo, D., Menegola, E., 1992. Effects of ethanol and acetaldehyde on rat embryos developing in vitro. In Vitro Cell. Dev. Biol. Anim. https://doi.org/10.1007/BF02631093.

Gofflot, G., Van Maele-Fabry, Picard, J.J., 1996. Cranial nerves and ganglia are altered after in vitro treatment of mouse embryos with valproic acid (VPA) and 4-en-VPA. Dev. Brain Res. https://doi.org/10.1016/0165-3806(96)00031-4.

Goncalves Leite, I.C., Koifman, S., 2009. Oral clefts, consanguinity, parental tobacco and alcohol use: a case-control study in Rio de Janeiro, Brazil. Braz. Oral Res. https://doi.org/10.1590/s1806-83242009000100006.

Haberland, M., Mokalled, M.H., Montgomery, R.L., Olson, E.N., 2009. Epigenetic control of skull morphogenesis by histone deacetylase 8. Genes Dev. https://doi.org/10.1101/gad.1809209.

Hudson, C., Schwanke, C., Johnson, J.P., Elias, A.F., Phillips, S., Schwalbe, T., Tunby, M., Xu, D., 2014. Confirmation of 6q21-6q22.1 deletion in Acro-cardio-facial syndrome and further delineation of this contiguous gene deletion syndrome. Am. J. Med. Genet. A. https://doi.org/10.1002/ajmg.a.36548.

JMPR, 2007. Report of the Joint Meeting of the FAO Panel of Experts on Pesticide Residues in Food and the Environment and the WHO Core Assessment Group on Pesticide Residues Geneva, Switzerland. 18–27 September 2007.

JMPR, 2004. Report of the Joint Meeting of the FAO Panel of Experts on Pesticide Residues in Food and the Environment and the WHO Core Assessment Group on Pesticide Residues Rome, Italy. 20–29 September 2004.

JMPR, 2010. Report of the Joint Meeting of the FAO Panel of Experts on Pesticide Residues in Food and the Environment and the WHO Core Assessment Group on Pesticide Residues Rome, Italy. 21–30 September 2010.

Knutson, S.K., Chyla, B.J., Amann, J.M., Bhaskara, S., Huppert, S.S., Hiebert, S.W., 2008 Apr 9. Liver-specific deletion of histone deacetylase 3 disrupts metabolic transcriptional networks. EMBO J 27 (7), 1017–1028. https://doi.org/10.1038/emboj.2008.51. Epub 2008 Mar 20.

Krauze, A.V., Myrehaug, S.D., Chang, M.G., Holdford, D.J., Smith, S., Shih, J., Tofilon, P.J., Fine, H.A., Camphausen, K., 2015. A phase 2 study of concurrent radiation therapy, temozolomide, and the histone deacetylase inhibitor valproic acid for patients with glioblastoma. Int. J. Radiat. Oncol. Biol. Phys. https://doi.org/10.1016/j.ijrobp.2015.04.038.

Kudoh, T., Wilson, S.W., Dawid, I.B., 2002. Distinct roles for Fgf, Wnt and retinoic acid in posteriorizing the neural ectoderm. Development.

Lagger, G1, O'Carroll, D, Rembold, M, Khier, H, Tischler, J, Weitzer, G, Schuettengruber, B, Hauser, C, Brunmeir, R, Jenuwein, T, Seiser, C, 2002 Jun. Essential function of histone deacetylase 1 in proliferation control and CDK inhibitor repression. EMBO J 321 (11), 2672–2681.

Lammer, E.J., Chen, D.T., Hoar, R.M., Agnish, Benke, P.J., Braun, J.T., Curry, C.J., Fernhoff, P.M., Grix, A.W., Lott, I.T., Richard, J.M., Sun, S.C., 1985. Retinoic acid embryopathy. N. Engl. J. Med. https://doi.org/10.1056/NEJM198510033131401.

Matsumoto, A., Nozaki, Y., Minami, T., Jimbo, E.F., Shiraishi, H., Yamagata, T., 2015. 6q21–22 deletion syndrome with interrupted aortic arch. Hum. Genome Var. https://doi.org/10.1038/hgv.2015.15.

Menegola, E., Broccia, M.L., Di Renzo, F., Prati, M., Giavini, E., 2000. In vitro teratogenic potential of two antifungal triazoles: triadimefon and triadimenol. In Vitro Cell. Dev. Biol. Anim. 36, 88–95. https://doi.org/10.1290/1071-2690(2000)036<0088:IVTPOT>2.0.CO;2.

Menegola, E., Broccia, M.L., Di Renzo, F., Giavini, E., 2001. Antifungal triazoles induce malformations in vitro. Reprod. Toxicol. https://doi.org/10.1016/S0890-6238(01)00143-5.

Menegola, E., Broccia, M.L., Di Renzo, F., Massa, V., Giavini, E., 2005a. Craniofacial and axial skeletal defects induced by the fungicide triadimefon in the mouse. Birth Defects Res. Part B Dev. Reproductive Toxicol. https://doi.org/10.1002/bdrb.20035.

Menegola, E., Di Renzo, F., Broccia, M.L., Prudenziati, M., Minucci, S., Massa, V., Giavini, E., 2005b. Inhibition of histone deacetylase activity on specific embryonic tissues as a new mechanism for teratogenicity. Birth Defects Res. Part B Dev. Reproductive Toxicol. https://doi.org/10.1002/bdrb.20053.

Menegola, E., Broccia, M.L., Di Renzo, F., Giavini, E., 2006. Postulated pathogenic pathway in triazole fungicide induced dysmorphogenic effects. Reprod. Toxicol. https://doi.org/10.1016/j.reprotox.2006.04.008.

Milstone, Z.J., Lawson, G., Trivedi, C.M., 2017. Histone deacetylase 1 and 2 are essential for murine neural crest proliferation, pharyngeal arch development, and craniofacial morphogenesis. Dev. Dynam. 246, 1015–1026. https://doi.org/10.1002/dvdy.24563.

Minoux, M., Rijli, F.M., 2010. Molecular Mechanisms of Cranial Neural Crest Cell Migration and Patterning in Craniofacial Development. Developmenthttps://doi.org/10.1242/dev.040048.

Montgomery, R.L., Davis, C.A., Potthoff, M.J., Haberland, M., Fielitz, J., Qi, X., Hill, J.A., Richardson, J.A., Olson, E.N., 2007 Jul 15. Histone deacetylases 1 and 2 redundantly regulate cardiac morphogenesis, growth, and contractility. Genes Dev. 21 (14), 1790–1802.

Montgomery, R.L., Potthoff, M.J., Haberland, M., Qi, X., Matsuzaki, S., Humphries, K.M., Richardson, J.A., Bassel-Duby, R., Olson, E.N., 2008 Nov. Maintenance of cardiac energy metabolism by histone deacetylase 3 in mice. J Clin Invest 118 (11), 3588–3597. https://doi.org/10.1172/JCI35847. Epub 2008 Oct 1.

Mossey, P.A., Little, J., Munger, R.G., Dixon, M.J., Shaw, W.C., 2009. Cleft lip and palate. https://doi.org/10.1016/s0140-6736(09)60695-4.

Mossey, P.A., Shaw, W.C., Munger, R.G., Murray, J.C., Murthy, J., Little, J., 2011. Global oral health inequalities: challenges in the prevention and management of orofacial clefts and potential solutions. Adv. Dent. Res. 23, 247–258. https://doi.org/10.1177/0022034511402083.

Murko, C., Lagger, S., Steiner, M., Seiser, C., Schoefer, C., Pusch, O., 2010. Expression of class i histone deacetylases during chick and mouse development. Int. J. Dev. Biol. 54, 1525–1535. https://doi.org/10.1387/ijdb.092971cm.

New, D.A., 1978. Whole-embryo culture and the study of mammalian embryos during organogenesis. Biol. Rev. Camb. Phil. Soc. https://doi.org/10.1111/j.1469-185x.1978.tb00993.x.

Nguyen, H.T.T., Sharma, V., McIntyre, R.S., 2009. Teratogenesis associated with

antibipolar agents. Adv. Ther. https://doi.org/10.1007/s12325-009-0011-z.
Oosterveen, T., Meijlink, F., Deschamps, J., 2004. Expression of Retinaldehyde dehydrogenase II and sequential activation of 5′ Hoxb genes in the mouse caudal hindbrain. Gene Expr. Patterns. https://doi.org/10.1016/j.modgep.2003.11.007.
Ornoy, A., 2009. Valproic acid in pregnancy: how much are we endangering the embryo and fetus? Reprod. Toxicol. https://doi.org/10.1016/j.reprotox.2009.02.014.
Osumi-Yamashita, N., 1996. Retinoic acid and mammalian craniofacial morphogenesis. J. Biosci. https://doi.org/10.1007/BF02703091.
Pautus, S., Aboraia, A.S., Bassett, C.E., Brancale, A., Coogan, M.P., Simons, C., 2009. Design and synthesis of substituted imidazole and triazole *N* -phenylbenzo[*d*]oxazolamine inhibitors of retinoic acid metabolizing enzyme CYP26. J. Enzym. Inhib. Med. Chem. 24, 487–498. https://doi.org/10.1080/14756360802218334.
PubChem [WWW Document].
RCSB PDB: Homepage [WWW Document].
Romitti, P.A., Herring, A.M., Dennis, L.K., Wong-Gibbons, D.L., 2007. Meta-analysis: pesticides and orofacial clefts. Cleft Palate-Craniofacial J. 44, 358–365. https://doi.org/10.1597/06-100.1.
Sabbagh, H.J., Hassan, M.H.A., Innes, N.P.T., Elkodary, H.M., Little, J., Mossey, P.A., 2015. Passive smoking in the etiology of non-syndromic orofacial clefts: a systematic review and meta-analysis. PloS One. https://doi.org/10.1371/journal.pone.0116963.
Senggen, E., Laswed, T., Meuwly, J.Y., Maestre, L.A., Jaques, B., Meuli, R., Gudinchet, F., 2011. First and second branchial arch syndromes: multimodality approach. Pediatr. Radiol. https://doi.org/10.1007/s00247-010-1831-3.
Sixto-López, Y., Gómez-Vidal, J.A., Correa-Basurto, J., 2014. Exploring the potential binding sites of some known HDAC inhibitors on some HDAC8 conformers by docking studies. Appl. Biochem. Biotechnol. 173, 1907–1926. https://doi.org/10.1007/s12010-014-0976-1.
Spilson, S.V., Kim, H.J.E., Chung, K.C., 2001. Association between maternal diabetes mellitus and newborn oral cleft. Ann. Plast. Surg. https://doi.org/10.1097/00000637-200111000-00001.
Suraweera, A., O'Byrne, K.J., Richard, D.J., 2018. Combination therapy with histone deacetylase inhibitors (HDACi) for the treatment of cancer: achieving the full therapeutic potential of HDACi. Front. Oncol. https://doi.org/10.3389/fonc.2018.00092.
Suuberg, A., 2019. Psychiatric and developmental effects of isotretinoin (retinoid) treatment for Acne Vulgaris. Curr. Ther. Res. Clin. Exp. https://doi.org/10.1016/j.curtheres.2019.01.008.
Trivedi, C.M., Luo, Y., Yin, Z., Zhang, M., Zhu, W., Wang, T., Floss, T., Goettlicher, M., Noppinger, P.R., Wurst, W., Ferrari, V.A., Abrams, C.S., Gruber, P.J., Epstein, J.A., 2007 Mar. Hdac2 regulates the cardiac hypertrophic response by modulating Gsk3 beta activity. Nat Med 13 (3), 324–331 Epub 2007 Feb 18.
Twigg, S.R.F., Wilkie, A.O.M., 2015. New insights into craniofacial malformations. Hum. Mol. Genet. https://doi.org/10.1093/hmg/ddv228.
Uehara, M., Yashiro, K., Mamiya, S., Nishino, J., Chambon, P., Dolle, P., Sakai, Y., 2007. CYP26A1 and CYP26C1 cooperatively regulate anterior-posterior patterning of the developing brain and the production of migratory cranial neural crest cells in the mouse. Dev. Biol. https://doi.org/10.1016/j.ydbio.2006.09.045.
UniProt [WWW Document].
Vujkovic, M., Ocke, M.C., Van Der Spek, P.J., Yazdanpanah, N., Steegers, E.A., Steegers-Theunissen, R.P., 2007. Maternal western dietary patterns and the risk of developing a cleft lip with or without a cleft palate. Obstet. Gynecol. 110, 378–384. https://doi.org/10.1097/01.AOG.0000268799.37044.c3.
Weichert, W., 2009. HDAC expression and clinical prognosis in human malignancies. Canc. Lett. https://doi.org/10.1016/j.canlet.2008.10.047.
Weston, J., Bromley, R., Jackson, C.F., Adab, N., Clayton-Smith, J., Greenhalgh, J., Hounsome, J., Mckay, A.J., Tudur Smith, C., Marson, A.G., 2016. Monotherapy treatment of epilepsy in pregnancy: congenital malformation outcomes in the child. Cochrane Database Syst. Rev. https://doi.org/10.1002/14651858.CD010224.pub2.
White, R.J., Schilling, T.F., 2008. How degrading: Cyp26s in hindbrain development. Dev. Dynam. https://doi.org/10.1002/dvdy.21695.
Wu, L., Chen, Z., Zhu, J., Hu, L., Huang, X., Shi, H., 2014. Developmental toxicity of organotin compounds in animals. Front. Mar. Sci. https://doi.org/10.3389/fmars.2014.00039.